VEGF-C ameliorates lymphatic drainage, portal pressure and ascites in experimental portal hypertension

Savneet Kaur[1*#], Dinesh M Tripathi[1*], Pinky Juneja, Impreet Kaur[1], Sumati Rohilla[1], Abhishak Gupta[1], Preety Rawal[1], Angeera Yadav[4], Archana Rastogi[2], SM Shasthry[3], V Rajan[3], VGM Naidu[4], Syed Nazrin Ruhina Rahman[5], Subham Banerjee[5#], Shiv K Sarin[3#].

[1]Department of Molecular and Cellular Medicine, Institute of Liver and Biliary Sciences, New Delhi

[2]Department of Pathology, Institute of Liver and Biliary Sciences, New Delhi

[3]Department of Hepatology, Institute of Liver and Biliary Sciences, New Delhi

[4]Department of Pharmacology and Toxicology, National Institute of Pharmaceutical Education and Research (NIPER)-Guwahati, Changsari-781101, Assam, India.

[5]Department of Pharmaceutics, NIPER-Guwahati, Changsari-781101, Assam, India.

*Shared first author

[#]Corresponding author

#Correspondence

Dr. Savneet Kaur, Assistant Professor, Department of Molecular and Cellular Medicine, Institute of Liver and Biliary Sciences, New Delhi, India, Phone no. 91-11-46300000, Email: savykaur@gmail.com

Prof. Shiv K Sarin, Director and Professor, Department of Hepatology, Institute of Liver and Biliary Sciences, New Delhi, India, Phone no. 91-11-46300000, Email: shivsarin@gmail.com

Dr. Subham Banerjee, Assistant Professor, Department of Pharmaceutics, NIPER-Guwahati, Changsari-781101, Assam, India, Email: banerjee.subham@yahoo.co.in

Conflict of Interest

The authors have declared that no conflict of interest exists.

Grant support:

The study was funded by Department of Science and Technology (DST), Ministry of Science & Technology, Government of India (DST/NM/NT/2019/191).

List of Abbreviations

VEGF-C: Vascular Endothelial Growth Factor-C; E-VEGF-C: Nanoengineered VEGF-C; Vegfr3: Vascular Endothelial Growth Factor Receptor 3; PDI: Polydispersity index; ZP: Zeta potential; D2 biopsy: Duodenal biopsy; CCl4: carbon tetra chloride; LyECs: lymphatic endothelial cells

Synopsis:

A lipid nanocarrier conjugated pro-lymphangiogenic molecule, VEGF-C with specificity for uptake by the gut lymphatic endothelial cells has been developed to enhance gut lymphangiogenesis. A targeted delivery of VEGF-C improves lymphatic vessel drainage, attenuating abdominal ascites and portal pressures. VEGF-C therapy holds immense potential to manage ascites in patients with decompensated cirrhosis having dilated gut lymphatic vessels.

Abstract

Background and aims: Gut lymphatic vessels are crucial in maintaining abdominal fluid homeostasis. An impaired lymphatic drainage of these vessels has been associated with the presence of ascites in liver cirrhosis. We thus explored the therapeutic effects of gut-targeted delivery of vascular endothelial growth factor-C (VEGF-C), a pro-lymphangiogenic factor, in cirrhosis and portal hypertension. ***Methods:*** Vegfr3 antibody-tagged lipocarriers were used to formulate E-VEGF-C molecule for its targeted delivery in lymphatic endothelial cells (LyECs). *In vitro* characterization, cytotoxicity, *in vivo* biodistrubution and pharmacokinetic analysis of E-VEGF-C was performed. *In vivo*, E-VEGF-C was given orally in cirrhotic and non-cirrhotic rat models of portal hypertension. Rats given lipocarriers alone served as vehicle. Mesenteric lymphatic vessels and drainage were analyzed. Ascites and hepatic hemodynamics was measured. Molecular and histological studies of the mesentery was performed. Lymphatic channels were also enumerated in duodenal (D2) biopsies from cirrhotic patients. ***Results:*** E-VEGF-C exhibited a size of <200nm and a zeta potential of 6mV. *In vitro* and *in vivo*, E-VEGF-C was efficiently taken up by mesenteric LyECs. E-VEGF-C treated rats displayed an increase in numbers and drainage of mesenteric lymphatic vessels and a reduction in ascites as compared to CCl4-vehicle. Portal pressures were attenuated in both cirrhotic and non-cirrhotic portal hypertensive rats treated with E-VEGF-C as compared to their respective vehicle. In patients', dilated lymphatic vessels were increased in decompensated as compared to compensated cirrhosis. ***Conclusion:*** A targeted mesenteric lymphangiogenesis leading to an improved lymphatic drainage may

serve as an emerging therapy for portal hypertension and ascites in patients with decompensated cirrhosis.

Keywords

Cirrhosis; Gut Lymphatic vessels; Lymphangiogenesis; Portal Hypertension; Targeted drug delivery

Introduction

Chronic liver diseases cause significant morbidity and mortality worldwide. They can progress from mild fibrosis to portal hypertension to cirrhosis, which may further proceed to end-stage liver disease with onset of decompensation (e.g. ascites) and finally development of hepatocellular carcinoma. Along-side other underlying factors, a deranged gut-liver axis plays a significant role in liver disease progression [1]. Whatever comes from the gut enters the liver through the portal circulation before returning to the heart via the hepatic vein. However, there exists a system of lymphatic channels in the gut, comprising of the intestinal and mesenteric lymphatic vessels that bypass the portal circulation in liver and directly connects the gut to the blood circulation via the thoracic duct. Gut lymphatics contain blind-ended lymphatic capillaries with a single layer of lymphatic endothelial cells (LyECs) in the duodenum (lacteals) while the contractile collecting vessels contain both the LyECs and smooth muscle cells in the mesentery [2]. Gut lymphatic vessels play essential roles in the absorption and transportation of fat, maintaining fluid homeostasis, removing interstitial fluid, macromolecules, immune cells, and microbial debris from the intestine and returning them to the blood circulation, thereby preventing edema and abdominal ascites [3].

Lymphangiogenesis in the gut during inflammation compensates for lymphatic insufficiency in patients with gut inflammatory diseases such as inflammatory bowel disease and Crohn's disease, where there is both an increase and redistribution of lymphatic vessels [4,5]. In liver cirrhosis, it is documented that the production of abdominal

lymph increases 30-fold and there exists a positive correlation of lymph flow with increasing portal pressures [6,7] .Using animal models of CCl4-induced liver damage, an elegant study has reported that mesenteric lymphatic vessels show an impaired phenotype and reduced contractility in cirrhosis [8].

VEGF-C, a key pro-lymphangiogenic factor primarily activates gut lymphangiogenesis via binding to its tyrosine kinase receptor, vegfr3 and the subsequent Akt pathway [9]. Lymphatic vessel markers such as vegfr3 and lyVE1 are strongly expressed in the branching vessels while podoplanin is expressed in the differentiated lymphatics in the gut [10]. Therapies aimed at enhancing lymphangiogenesis and improving the lymphatic transport and function with pro-lymphangiogenic factors, such as VEGF-C has been shown to constitute an effective strategy to improve lymphatic drainage and ameliorate inflammation in diseases like rheumatoid arthritis, skin inflammation and hepatic encephalopathy [11–14]. Use of pro-lymphangiogenic factors as therapeutic molecules for the restoration of gut lymphatic drainage in cirrhosis has however not been explored. The short half-life and systemic side effects of these growth factors are some of the major hurdles that have limited their applications in the clinical arena [15].

In the current study, we hypothesized a therapeutic role of pro-lymphangiogenic factor, VEGF-C in portal hypertension. To minimize the side effects of systemic delivery and increase the gut bioavailability of VEGF-C, we fabricated an engineered human VEGF-C gene by encapsulating it within lipocarriers and coating it with lymphatic vessel marker, vegfr3 antibody to ensure its lymphatic vessel-specific delivery for targeted gut lymphangiogenesis. We studied the effects of this synthesized VEGF-C molecule on lymphatic vessels and lymphatic drainage in the mesentery, abdominal ascites, hepatic

and systemic hemodynamics and liver pathology in experimental models of liver cirrhosis and portal hypertension.

Results

E-VEGF-C for sustained and targeted delivery of VEGF-C in Vegfr3+ lymphatic endothelial cells

Given the fact that there exists a lymph transport failure of the mesenteric lymphatic channels in experimental cirrhosis with ascites [8], we hypothesized that enhancing the number of functional lymphatic vessels in the mesentery by treating with lymphangiogenic factor, VEGF-C may improve lymphatic drainage in cirrhotic rats. To this end, we developed human VEGF-C plasmid encapsulated inside the lipocarriers (Figure 1A). The lipocarriers were prepared with soya phosphatidylcholine (SPC) with the addition of stearylchloride (SC). After encapsulation, VEGF-C lipocarriers were conjugated with lymphatic endothelial receptor antibody, vegfr3 to specifically achieve delivery and internalization of VEGF-C in vegfr3-positive lymphatic endothelial cells. Vegfr3 has been reported to be exclusively expressed in the lymphatic vessels [16]. In dynamic light scattering (DLS) analysis, the z-average particle size of engineered VEGF-C (E-VEGF-C) was found to be 110.7 nm with a polydispersity index (PDI) value of 0.272 (Figure 1B). The zeta potential value of the E-VEGF-C-engineered immunolipo-nanocarriers before vegfr3 antibody incubation was found to be almost neutral (+1.12 mV) but slightly inclined towards positive surface charge value (+6.52 mV), after vegfr3 antibody attachment (Figure1C, D). The scanning electron microscope (SEM) image of E-VEGF-C immunolipocarriers images indicated cluster form of particles in nanoformat with desired size range (Figure 1E). The immunolipocarriers could be seen forming agglomerates or lipid clusters due to sticky nature of lipoid S75 soybean phospholipids with 70% phosphatidylcholine. Transmission electron microscope (TEM) analysis of E-

VEGF-C immunolipocarriers revealed them as irregular and scattered nanoparticles with desired nano size range below 200nm (Figure 1F). These observations were in accordance to DLS analysis.

To ensure if E-VEGF-C is internalized into the rat mesenteric LyECs *in vitro*, we first isolated and sorted the podoplanin (pdpn+) and CD31+ LyECs from rat mesenteric tissues. In the flow sorting assays, of the total population of cells, we obtained around 2.1 % population of pdpn+ and CD31+ LyECs (Supp Figure S1A). This population when cultured on fibronectin coated plates stained intensely with pdpn antibody, confirming their phenotype (Figure 2A, B). The LyECs were incubated with green coumarin-6-labelled E-VEGF-C. Fluorescence microscopy revealed an efficient internalization of E-VEGF-C (about 90%) by the LyECs at 4 h (Figure 2C, D).

Tissue Bio-distribution of E-VEGF-C *in vivo*

To investigate the specificity of E-VEGF-C delivery *in vivo*, tissue biodistribution studies of E-VEGF-C were performed two hours post its oral administration by using spectroflourimetry, fluorescence microscopy and human VEGF-C ELISAs in control and cirrhotic rats (Figure 3A). The lipid format, attached vegfr3 antibody along with an oral administration of E-VEGF-C enhanced the targeted delivery of VEGF-C into the gut lymphatic vessels. Some amount of fluorescence was observed in almost all tissues in both control and CCl4 rats (Supp Figure 2A-C). In the CCl4 animals, the *in vivo* staining showed a co-localization of the coumarin-6 tagged nanoparticles with LyEC-specific marker, pdpn, indicating a targeted delivery in these cells (Figure 3B). CCl4 cirrhotic rats also showed increased levels of human VEGF-C levels in the mesenteric and duodenal

tissues in comparison to the control animals (Figure 3B, C $P < 0.05$ each). The human VEGF-C levels were also detected in other tissues besides duodenum and mesentery in both control and CCl4 rats, which might be due to the detection of endogenous rat VEGF-C levels by the ELISA kit (Figure 3C). In serum of CCl4 animals, levels of VEGF-C exhibited a biphasic peak, the first peak appeared at about 10 min, and the second peak at about 5 hours (Figure 3D). There was no adverse effect or mortality after E-VEGF-C treatment in either control or CCl4 rats.

E-VEGF-C treatment induces Lymphatic Vessel Proliferation and Improves Drainage

We next studied the effects of E-VEGF-C treatment in the mesenteric lymphatic vessels in the cirrhotic animals (Figure 4A). Both CCl4-V cirrhotic and E-VEGF-C rats showed significantly increased numbers of pdpn+ lymphatic vessels in the mesenteric tissues as compared to the control rats, which had negligible pdpn staining (Figure 4B, C). Interestingly, H & E of the mesenteric tissues also revealed a reduction in the inflammation in the E-VEGF-C rats in comparison to that seen in the vehicle animals (Supp Figure S3). Staining of the mesenteric tissues for vegfr3 clearly showed a markedly enhanced number of these branching vessels in the E-VEGF-C treated animals as compared to that of the vehicle (Figure 4D, E). We next analyzed the protein expression of human VEGF-C protein in the mesenteric tissues in different study groups. Results showed a significant increase in VEGF-C protein in the treated tissues as compared to the vehicle treated tissues. To investigate active lymphangiogenesis in the mesenteric tissues, we studied expression of the Akt/pAkt and pERK/ERK protein that

act downstream of vegfr3 pathway. As compared to the controls, the p-Akt/t-Akt was enhanced in both the vehicle and E-VEGF-C rats while that of pERK/ERK was substantially enhanced in the treated animals in comparison to that observed in vehicle animals, indicating an activation of the lymphangiogenic pathways downstream of vegfr3 (Figure 4F). To assess lymphatic drainage, we studied the functionality of the lymphatic vessels by measuring the amount of gavaged bodipy flourescence in the mesenteric vessels in the study groups. E-VEGF-C treated CCl4-V rats revealed a significant increase in flourescence as compared to that seen in the vehicle rats with respect to the controls ($P< 0.001$, Figure 4G, H).

E-VEGF-C reduces Ascites and ameliorates Portal Pressure in Cirrhotic and Non-Cirrhotic Portal Hypertensive Rats

We then investigated whether an improvement in lymphatic drainage and a reduction in mesenteric inflammation was associated with a reduction in ascitic fluid volume in the E-VEGF-C treated cirrhotic rats. No ascites was observed in the control group, whereas all the CCl4-V cirrhotic rats displayed severe ascites in our study. At the end of treatment, we assessed the volume of peritoneal fluid in the CCl4-V and E-VEGF-C groups. E-VEGF-C rats displayed a marked reduction in the ascites volume as compared to that observed in CCl4-V rats as was also clearly evident in CT scan slices of the two groups ($P< 0.001$, Figure 5A, B, Supp Table S3). Along with ascites reduction, evans blue analysis showed a significant increase in plasma volume in cirrhotic rats treated with E-VEGF-C compared with vehicle animals ($P< 0.05$, Figure 5C).

Next, we analyzed if this reduction in the ascitic fluid volume after E-VEGF-C treatment was also associated with changes in liver physiology and pathology. Intraperitoneal CCl4 treatment for 10 weeks markedly increased portal pressure (PP) in the rats in comparison to that of the control rats (Figure 5D). E-VEGF-C treatment, however significantly attenuated the PP as compared to the vehicle treated rats ($P< 0.001$, Figure 5D). To ascertain if the observed reduction in PP was due to a change in the portal blood flow (PBF) or intrahepatic resistance (IHR), we also monitored these parameters in all the study groups. E-VEGF-C treatment significantly decreased the PBF, in turn increasing the mean arterial pressure (MAP) as compared to that of the CCl4-V cirrhotic rats (Figure 5D, Supp Figure S4). The IHR in E-VEGF-C treated rats was however similar to that of the cirrhotic rats. In comparison to control rats, liver weights in E-VEGF-C rats and CCl4-V rats were also similar (Supp Figure S4). We next evaluated changes in histological and biochemical parameters of liver in the cirrhotic animals. Masson's trichrome staining of the liver tissues revealed that both E-VEGF-C and vehicle rats showed Ishak's fibrosis scores of 5/6 or 6/6 depicting complete cirrhosis (thick fibrous septa or many minute nodules) (Figure 5E). In terms of biochemical parameters, CCl4 treatment resulted in a significant increase in serum ALT levels and a decrease in albumin levels as compared to the control group (Supp Table S3). There was no significant improvement in levels of serum albumin and ALT in the E-VEGF-C treated rats as compared to that seen in CCl4 rats. The kidney functions tests were in normal ranges in all the study groups (Supp Table S3).

Next, we investigated the expression of important genes known to be associated with VEGF-C expression in the mesentery. Of all the genes analyzed, mesenteric tissues in E-

VEGF-C treated rats showed a marked increment in the expression of the chemokine, CCL21 ($P < 0.05$, Figure 5F). Interestingly, the pro-inflammatory gene, iNOS instead showed a significant reduction in their expression in E-VEGF-C treated rats in comparison to that observed in the CCl4-V rats ($P < 0.05$ for each, Figure 5F).

We also assessed levels of TNF-α and endotoxins in the ascitic fluid and in the serum. Serum endotoxins and TNF-α levels were considerably enhanced in CCl4-V cirrhotic rats in comparison to that present in control rats (Supp Figure S5A, B). We did not observe any significant change in the serum endotoxin and TNF-α levels in the E-VEGF-C treated rats in comparison to that observed in the CCl4-V rats (Supp Figure S5A, B). In the ascitic fluid, there was a significant decrease in the levels of endotoxins per ml in the E-VEGF-C treated rats vis a vis CCl4-V cirrhotic rats (Supp Figure S5C). A substantial reduction in the ascitic fluid volume per se in E-VEGF-C treated rats might have also resulted in an overall decrease in the levels of both endotoxins and TNF-α in the abdomen. Since VEGF-C also participates in blood vessel angiogenesis in some tissues, we also evaluated if E-VEGF-C had any effects on the mesenteric tissue blood vessels and inflammation. We did not find any significant difference in the number of CD31-positive vessels between CCl4-V and E-VEGF-C rats (Supp Figure S6A, B).

E-VEGF-C reduces Portal Pressure in Non-Cirrhotic Portal Hypertensive Rats

We next probed if E-VEGF-C treatment improved PP irrespective of liver cirrhosis, by measuring the hepatic hemodynamics in non-cirrhotic portal hypertensive (PPVL) animals (Figure 6A). Histology of these animals displayed portal inflammation in liver

but no significant fibrosis (Supp Figure S7). In the mesentery, E-VEGF-C treated PPVL rats showed an increased presence of vegfr3+ lymphatic vessels and reduced inflammation vis-à-vis the PPVL vehicle animals (Figure 6B, C, Supp Figure S7). PPVL animals treated with E-VEGF-C also displayed an increased VEGF-C and pERK/ERK protein expression in comparison to that seen in the vehicle rats (Figure 6D). Hemodynamic analysis depicted a significant reduction in the PP and PBF of PPVL animals treated with E-VEGF-C in comparison to that observed in vehicle animals ($P< 0.001$, Figure 6E). The expression of bFGF, CCL21, iNOS and eNOS was significantly higher in the mesentery of the PPVL vehicle animals in comparison to the controls (Figure 6F). In E-VEGF-C treated PPVL rats, there was a significant reduction of iNOS as compared to the vehicle animals ($P< 0.05$, Figure 6F).

Vegfr3+ lymphatic vessels are dilated in patients with decompensated cirrhosis

To study the clinical relevance of gut lymphatic vessels and liver cirrhosis, we investigated some of the duodenal (D2) biopsies of cirrhotic patients (both compensated and decompensated). Characteristics of the patient groups are summarized in Table 1. All patients with decompensated cirrhosis had ascites, whereas ascites was absent in all patients diagnosed with compensated cirrhosis. None of the patients had chylous ascites. The lymphatic vessels in patients were characterized by H & E and vegfr3 and pdpn staining of the D2 biopsies.

Histologically, patients with decompensated cirrhosis displayed a large number of dilated lymphatic channels (consisting of a single layer of endothelial cells) in comparison to patients with compensated cirrhosis or healthy controls (Supp Figure 8). Both pdpn and

vegfr3 protein expression was evident in the lymphatic vessels and was markedly increased in decompensated as compared to compensated cirrhosis (Figure 7A-C). Intriguingly, a marked dilation of vegfr3-positive lymphatic vessels was observed in the mucosal and submucosal regions in biopsies of decompensated cirrhosis compared to the controls and compensated cirrhosis (Figure 7D).

Discussion

A previous study in cirrhotic rats documented that an increased expression of eNOS in the mesenteric LyECs was the cause of dysfunctional and dilated lymphatics in cirrhosis and that inhibiting eNOS improved the lymphatic transport of the existing vessels by increasing contractile activity of these vessels [8]. In our study, instead of manipulating the contractile activity of the existing mesenteric lymphatic vessels by using an eNOS inhibitor, we focused on increasing the numbers of new lymphatic channels via VEGF-C treatment. To minimize the systemic toxic effects of VEGF-C, we designed the therapeutic VEGF-C molecule by using nanolipocarriers. A recent report illustrated the therapeutic potential of the fully human fusion protein, F8-VEGF-C (VEGF-C linked to F8 antibody) for a targeted delivery of VEGF-C in mouse models of chronic inflammatory skin disease. However, the study did not report a sustained release of VEGF-C [17]. We used various strategies in this study to ensure a targeted and sustained delivery of VEGF-C in the lymphatic channels. Firstly, the use of lipid nanocarriers might have allowed the VEGF-C cargo to be carried in the chylomicron size particles in the lymphatic vessels after an oral delivery. The encapsulation also ensured its release in a sustained and programmable manner [18]. Secondly, the use of vegfr3 antibody coating increased the likelihood of a targeted delivery of VEGF-C to the gut LyECs. The *in vitro* uptake studies clearly depicted more than 90% uptake of the E-VEGF-C by the mesenteric LyECs. We did not follow any conjugation chemistry for the preparation of the E-VEGF-C molecule, rather we focused on the preparation of simple solid lipid nanoparticles with an aqueous template using modified multiple emulsification technique as previously reported [19].

In the *in vivo* biodistribution studies, cirrhotic rats had maximum levels of E-VEGF-C in the mesenteric tissues. In the plasma, VEGF-C release pattern in the formulation followed a biphasic release behavior. The initial burst release of the drug observed at 10 min might be due to presence of adsorbed drug on the surface of nanoparticles, while the second peak at 5 h, depicting sustained release of drug might be due to increased diffusional distance and hindering effects by the surrounding solid lipid shell.

Treatment with E-VEGF-C markedly enhanced the expression of VEGF-C proteins in the mesentery, indicating VEGF-C-driven proliferation in the LyECs. Functionally, both MAP/ERK and PI3k/Akt pathways play important roles in regulating the sprouting and proliferation/survival of LyECs respectively [20]. We observed a predominance of the MAP/ERK pathway over the Akt pathway participating in the lymphatic vessel proliferation in the mesenteric tissues of the treated animals [20]. Also, our treatment significantly improved the lymphatic drainage of the vessels. This is in accordance with many previous studies that have shown drainage-promoting function of VEGF-C in experimental models of bacterial skin inflammation and inflammatory bowel disease [21,22]. An improvement in lymphatic drainage and functionality of the new vessels in CCl4 cirrhotic rats formed was well evident by a marked reduction in the ascitic fluid volume in rats with fully developed ascites. A decrease in ascites was accompanied by an increase in the plasma volume of the treated rats suggesting that there may be reabsorption of ascites into the circulating blood [7]. Along with a reduction in ascites, there was also a significant decrease in the PP in cirrhotic portal hypertensive rats treated with E-VEGF-C, which was associated with attenuated PBF and increased MAP. There was however no change in the IVR, indicating that attenuation in PBF and not the hepatic

resistance (fibrosis) led to an improvement in portal pressure after treatment. A decrease in PP may be caused by a reduction in the intra-abdominal pressure that might have occurred during removal of ascitic fluid into newly formed lymphatic vessels. It has been postulated that removal of ascites plays a role in the postparacentesis systemic hemodynamic changes through mechanical decompression of the splanchnic vascular bed [23]. However, a reduction in PP due to an increase in the number of lymphatic vessels and a decrease in the interstitial fluid pressure may also have led to a decrease in ascites [24]. The decrease in PP observed in the non-cirrhotic PPVL animals after E-VEGF-C treatment validated the favorable effects of the pro-lymphangiogenic treatment on PBF and systemic hemodynamics. An improvement in the PP was not associated with a significant improvement in liver pathology in the treated cirrhotic rats, stipulating that there are no direct protective effects of E-VEGF-C treatment on the hepatic compartment per se.

Mesenteric angiogenesis marked by an increase in CD31+ vessels is a common feature of cirrhosis, and this was also observed in cirrhotic rats [25]. However, we did not detect any significant changes in the density of CD31+ blood vessels in E-VEGF-C–treated cirrhotic rats, reflecting that VEGF-C did not affect the mesenteric blood vessels analogous to that has been documented earlier [21,22]. With respect to inflammation, there was a conspicuous decrease in mesenteric tissue inflammation in histological analysis in both cirrhotic and non-cirrhotic rats. The mesenteric expression of pro-inflammatory genes such as iNOS was also downregulated after E-VEGF-C treatment in both cirrhotic and PPVL animals. It has been reported formerly that during inflammation an increase in iNOS-expressing inflammatory cells significantly reduce lymphatic contraction [26,27]. Most striking was the

increase in the gene expression of CCL21 in E-VEGF-C rats in the mesentery, demonstrating that the newly formed lymphatic vessels might also be capable of augmenting the production of chemoattractants. An earlier study documented that stimulation of cardiac lymphangiogenesis with VEGF-C improved the trafficking of immune cells to draining lymph nodes after myocardial infarction [28]. It would be worthwhile to study underlying mechanisms of immune modulation and inflammation in the mesenteric tissues and lymph nodes by VEGF-C treatment in these animal models.

With respect to eNOS, previous studies have illustrated an increase in the expression of phosphorylated eNOS due to an activation of PI3Kinase/Akt signaling in LyECs after VEGF-C treatment [29]. Also, eNOS inhibition has shown to cause a decreased lymphatic fluid velocity, and NO donors have a favorable effect specifically on the collecting lymphatic vessels [30]. We did not observe a significant change in the eNOS gene expression in the treated animals but a limitation of our study is that we have not estimated the eNOS signaling pathway specifically in the LyECs after VEGF-C treatment, which thus warrants further investigations. In this regard, it would also be interesting to evaluate the precise effects of eNOS activators such as statins, that attenuate hepatic microvascular dysfunction, on the mesenteric lymphatic vessels and drainage in portal hypertension [8,31].

We also observed significantly increased number of dilated vegfr3+ and pdpn+ duodenal lymphatic vessels in patients with decompensated cirrhosis with both mucosal and submucosal involvement, clearly implying gut lymphatic dysfunction similar to that seen in intestinal lymphangectasia and gut inflammatory disorders [5,32]. An increase in the expression of vegfr3-postive duodenal vessels in patients with decompensated cirrhosis

may be attributed to compensatory lymphangiogenesis response by the gut lymphatic vessels to accommodate an increased interstitial fluid [33,34]. More importantly, the co-existence of ascites and significantly increased dilated lymphatic channels in the decompensated patients underscore the fact that an impairment of gut lymphatic function and drainage might represent one of the key factors affecting fluid accumulation into the peritoneal cavity in cirrhosis [7]. It would be informative to correlate the grade and severity of ascites with the number of dilated duodenal lymphatic channels in a larger group of decompensated cirrhotic patients.

To summarize, our study underscores the use of a VEGF-C as a lymphangiogenic growth factor for enhancing mesenteric lymphangiogenesis. The study proposes pro-lymphangiogenesis as an innovative and targeted strategy for the management of ascites and portal hypertension.

Materials and Methods

Preparation and Characterization of Engineered VEGF-C

Materials: Stearyl chloride (SC), Tween 80, and Coumarin-6 were procured from Sigma-Aldrich Chemical, St. Louis, USA. pQCXIP-VEGFC was a gift from Michael Grusch (Addgene plasmid # 73012; http://n2t.net/addgene:73012; RRID:Addgene_73012), respectively. Polyclonal vegfr3 antibody was procured from Thermofisher scientific, Massachusetts, USA. Fat free soybean phosphatidylchloline (SPC) was obtained as a gift sample from Lipoid GmbH, Ludwigshafen, Germany. All other chemicals and solvents were of analytical reagent grade and used as received. Double distilled water was used throughout the experiment.

Preparation of E-VEGF-C immunolipo-nanocarriers: Vegfr3 antibody tagged E-VEGF-C immunolipocarriers (E-VEGF-C) were formulated using cold high shear homogenization (HSH) technique using digital HSH. VEGF-C was encapsulated inside the amphiphilic core of SPC and primary emulsion was prepared by adding this into SC matrix under gentle stirring. This primary water-in-oil (w/o) emulsion was further then transferred into secondary cold aqueous phase to form w/o/w type emulsion under high-shear homogenization (T-18 Digital Ultra-Turrax®, IKA India Pvt. Ltd., Bengaluru, India). The obtained nanodispersions were kept at 4°C for further analysis. VEGF-C-engineered lipo-nanocarriers dispersion was incubated in vegfr3 primary antibody (50 ng/µL in Tris-EDTA buffer) for 24 hours at 4°C temperature in order to finally obtain E-VEGF-C for a targeted gut lymphatic vessel delivery. For tissue biodistribution studies, VEGF-C was engineered using coumarin-6 dye labelled SC.

DLS, SEM and TEM analysis: Before and after Vegfr3 incubation, E-VEGF-C immunolipo-nanocarriers dispersion were evaluated for mean particle size (z-average), PDI and zeta potential analysis by dynamic laser light scattering (DLS) method using Zetasizer (Nano ZS-90, Malvern Instruments, UK). Surface topography of E-VEGF-C immunolipocarriers dispersion were viewed under scanning electron microscope (SEM) examination. Surface morphology and size of E-VEGF-C was also examined under a transmission electron microscope (TEM) with an acceleration voltage of 100 kV.

***In vivo* studies**

Study Groups and treatment: All animals received humane care according to the criteria outlined in the ‘‘Guide for the Care and Use of Laboratory Animals’’ prepared by the National Academy of Sciences and published by the National Institutes of Health (NIH publication 86-23 revised 1985). The study performed was duly approved by the Animal ethics committee of ILBS, New Delhi as per the standard guidelines (Ethics Protocol No: IAEC/ILBS/18/01). Rats were housed in a room at 22 ± 3^0C and 12 hours light dark cycle and were given food and water ad libitum. Studies were performed on thirty-six 8-week old male Wistar rats and twelve male 8-10 week old Sprague Dawley (SD) rats, weighing 250~300 g. Wistar rats were used for developing cirrhotic models of portal hypertension while SD rats were utilized for development of non-cirrhotic portal hypertension models by partial portal vein ligation (PPVL). Animals were randomized in three groups for the cirrhotic study: Healthy Control group (treated with saline), CCl4-V or vehicle group (CCl4 plus lipid nanocarriers alone without VEGF-C and vegfr3 Ab) and E-VEGF-C group (CCl4 plus E-VEGF-C). Cirrhosis was induced by intraperitoneal

injection of 1.0 ml/kg body weight of 10% CCl4 in olive oil, three times a week for 10 weeks. The control group (control) received olive oil 1.0 ml/kg intraperitoneal injection (i.p.) three times a week for 10 weeks and then saline 1.0 ml/kg per oral 3 days a week during the 11th week (control, n= 8). The vehicle group (CCL4-V) received CCl4 1.0 mg/kg, i.p. three times a week for 10 weeks and then lipid nanocarrier formulation (without VEGF-C plasmid) via oral administration 3 days a week during the 11th week (vehicle, n= 8). The E-VEGF-C group, along with CCl4, received E-VEGF-C through the oral route at a dose of 300 μg of the construct per kg body weight of the animal, via 3 injections during the 11th week (n=8). All CCl4 animals had fully developed cirrhosis and ascites after 10 weeks. Ascites was graded as mild, moderate or severe based on the fluid volume. Less than 1ml was mild, 1-4ml was moderate and >4ml was severe. These rats were sacrificed after 11 weeks, 48 hours after the last dose of saline, vehicle or E-VEGF-C, after performing the hemodynamic studies.

Two groups were prepared in PPVL study. PPVL-vehicle (PPVL plus nanocarriers alone) and PPVL-E-VEGF-C (PPVL plus E-VEGF-C). Non-cirrhotic animal models of portal hypertension were developed by partial portal vein ligation (PPVL) as previously described [35]. Briefly, under isoflurane anesthesia, using a single ligature of 3-0 silk tied around the portal vein, a calibrated constriction was done with a 19-gauge blunt-tipped needle. The needle was then removed, leaving a calibrated constriction of the portal vein. In PPVL animals, two groups were randomized. In the PPVL + vehicle group, lipid nanocarrier formulation (without VEGF-C plasmid) was administered orally via 3 injections in 3 days one day after the PPVL surgery week (PPVL vehicle, n= 6). In PPVL plus E-VEGF-C group, E-VEGF-C was orally given at a dose of 300 μg of the construct

per kg body weight of the animal, via 3 injections in 3 days one day after the PPVL surgery week (PPVL plus E-VEGF-C, n= 6). In a few rats, plasma volume was measured using Evans Blue dye.

***In vivo* biodistribution and half-life studies:** , E-VEGF-C (single dose: 300 μg/kg) tagged with coumarin-6 dye was administered at day 0 in healthy control animals and in CCL4 rats after 10 weeks. Rats were euthanized after 2 hours of single E-VEGF-C oral administration, for collection of liver, intestine, mesentery, spleen, lung and kidney tissues. The tissues were weighed and homogenized with physiological saline and the fluorescence intensity was detected at 520nm using a spectroflourimeter. Some part of the tissues was also observed under a florescence microscope for visual detection of labeled nanoparticles. The fluorescence intensity values of coumarin were normalized with that of control rats without any treatment. Levels of VEGF-C were determined per mg protein of the tissues by using the human VEGF-C ELISA kit (elabsciences, Houston, USA) according to the manufacturer's protocol.

For plasma half-life studies, after single oral injection of E-VEGF-C, serial blood samples (300 μl) were taken in EDTA vials from the rats at 10 min, 20 min, 30 min, 1 h, 5 h, 10 h and 24 h. After 20 minutes of incubation at room temperature, the blood samples were centrifuged at 1200 *g* for 10 minutes. The plasma (100-150 μl) were collected, snap frozen, and stored at –80°C. The amount of VEGF-C in each sample was determined using the human VEGF-C ELISA Kit as before. The plasma VEGF-C concentration–time data was analyzed at different time points.

Analysis of Plasma Volume: Plasma volume was measured using Evans Blue dye, as previously described [8]. Briefly, 0.2 ml of Evans Blue (Himedia labs) solution (3 mg) was

injected through a jugular vein catheter followed by saline to clear the dye from the catheter. After five, 1 ml of blood was withdrawn from a femoral artery catheter. The plasma aliquot was diluted ten times in distilled water, and the absorbance was read at 600-nm by a spectrophotometer. The plasma volume (ml) was calculated by using the formula:

Plasma volume (ml) = Absorbance of standard/Absorbance of sample x 10, where the standard was 3 mg of Evans Blue dye in 10 ml of plasma diluted by a factor of 10

Analysis of Lymphatic Transport using Tracer: To evaluate lymphatic drainage in the mesenteric lymphatic vessels in different study groups of cirrhotic animals, a long-chain fatty acid (bodipy), a lymphatic tracer was administered intragastrically in few animals of the three treated groups (n= 4 each). After 2 hours, fluorescent images of the mesenteric lymphatic drainage were obtained using fluorescence microscopy. Six-eight fields from each slide were randomly selected, and photographs were taken using a confocal microscope (Nikon Confocal A1r system, Nikon Instruments Inc., Tokyo, Japan). Quantification of the bodipy fluorescence was also done by measuring the fluorescence intensity in the green channel by NIS Elements ver 4.0. The fluorescence intensity values of bodipy were normalized with that of rats without any oral gavage of bodipy.

Assessment of Hepatic and Systemic Hemodynamic Parameters: Rats were anesthetized with ketamine hydrochloride (60 mg/kg) plus midazolam (3mg/kg) intraperitoneally, fastened to a surgical board, and maintained a constant temperature of 37°C ± 0.5°C. Tracheostomy and endotracheal cannulation (PE-240 catheter; Portex, Minneapolis, MN) was performed to maintain adequate respiration during anesthesia. The femoral artery and the ileocolic vein were cannulated with PE-50 catheters to

measure mean arterial pressure (mm Hg) and portal pressure (PP) (mm Hg), respectively. A nonconstrictive perivascular ultrasonic transit time flow probe (2PR, 2-mm diameter; Transonic Systems Inc., Ithaca, NY, USA) was placed around the portal vein as close as possible to the liver to measure portal blood flow (PBF) (mL/min). Intra hepatic vascular resistance (IHR) (mm Hg·mL·min^{-1}·g^{-1}) was calculated as PP/PBF. Blood pressures and flows were registered on a multichannel, computer-based recorder using Chart, version 5.0.1, for Windows software (PowerLab; AD Instruments, New Delhi, India). Hemodynamic data were collected after a 20-minute stabilization period

Computed tomography analysis: Computed tomography (CT) examination was performed 48 h after the treatment to visualize ascites and validate the presence of decompensation in cirrhotic animals. The animals were evaluated using Somatom Definition AS plus 128 Acquisition 384 slice reconstruction (Siemens Healthineers, Forchheim, Germany).

***In vitro* Studies with LyECs**

Isolation of Lymphatic endothelial cells from mesenteric tissue of rat and uptake of E-VEGF-C in vitro

For isolation of mesenteric LyECs, the rat was anesthetized with ketamine xylazine cocktail. A mid-line incision was done to perfuse mesentery with saline by inserting the catheter into the ilio-caecum vein [8]. Clear mesentery tissue was extracted and placed in DMEM supplemented with 2% antibiotic and antimycotic solution. Sterile scissor was used to finely mince the tissue into ~1 mm3 pieces. Minced tissue was centrifuged at 2500 rpm for 10 min at RT and washed twice with PBS. For in vitro digestion, 0.25% collagenase IV was previously prepared and prewarmed at 37 C. Tissue was resuspended

in enzyme solution supplemented with 3mM CaCl2 at constant shaking for proper digestion. Following digestion for 30 minutes at 37 C, the tube was then transferred to the biosafety cabinet and passed the digested tissue suspension through a 70 μm strainer placed into a sterile 50 ml tube. An equal amount of sterile DMEM media was passed through a strainer to inactivate the enzyme. The cell suspension was then centrifuged at 1200 rpm for 5 min at 4 C and washed twice with PBS. Cell pellet was resuspended in the complete endothelial cell growth medium (EGM) and seeded on precoated fibronectin plates. The cells were incubated overnight at 37 C in 5% CO2. Media was changed after 12 hrs.

For sorting of LyECs, LyEC-specific primary antibody podoplanin (pdpn, 1:200 dilution) and CD31 (1:100 dilution) was added in the cell suspension, and cells were incubated on ice for 30 mins. After washing, the secondary antibody conjugated with fluorochrome was added in 1:500 dilution and incubated on ice for 30 min. Thereafter, sorting was done in sterile conditions using FACS sorter and cells were collected in EGM-2 media. After sorting, the cells were washed with PBS, resuspended in EGM-2 media, and seeded on precoated fibronectin plates. The cultured cells were incubated with nanoengineered VEGF-C particle for 30 mins at 37 C in 5% CO2. After incubation, cells were rinsed 3 times with PBS to washout the remaining nanoparticle. Cells were then fixed for 7 min at room temperature in the dark, using a permeabilization and fixing kit (BD Cytofix/Cytoperm) and washed one time with BD perm/wash buffer [18]. Staining was done with DAPI (4,6-diamidino-2-phenylindole) in 1:2000 dilution. Fluorescence of coumarin-6 labeled VEGF-C particle and DAPI stained cells were imaged using an

inverted fluorescence microscope (Evos microscope) in the green and blue channels, respectively. Flourescence was quantified with ImageJ software.

Assessment of blood and lymphatic vessels by immunohistochemistry and immunoflourescence: Intestinal (patients) and mesenteric tissue samples (animals) were fixed in 10% buffered formaldehyde solution and embedded in paraffin. Immunolabelling was performed using specific antibodies for blood vessel marker (CD31), lymphatic endothelial markers, vegfr3, and pdpn. Thereafter, the samples were either incubated with PolyExcel HRP labeled polymer and DAB substrate or secondary fluorescent antibodies. Immunolabelled cells were detected using a light or fluorescence microscope accordingly. In vivo tracking of the coumarin-6 lableed E-VEGF-C in the lymphatic endothelial cells was done by pdpn fluorescence staining of the mesenteric tissues 2h post oral treatment. Six-eight fields from each slide were randomly selected, and photographs were taken using an inverted fluorescent microscope (Nikon Instruments, Inc) and quantified with Image J software. Details of the antibodies are given in Supp Table S2.

Detection of TNF-α and endotoxins in the Ascitic fluid and Systemic Circulation: The levels of TNF-α was assessed using TNF-α ELISA kit (Thermofisher scientific, Massachusetts, USA) as recommended by the manufacturer's protocol. Endotoxin levels in the serum were assessed by a chromogenic kinetic limulus ameobocyte lysate assay kit following the manufacturer's instructions **(**Thermofisher scientific, Massachusetts, USA).

RNA extraction and RT-PCR: RNA extraction and RT-PCR was done from excised the mesenteric tissues stored in RNA later buffer. Total RNA was isolated by using Nucleopore kit as per manufacturer's instructions. RNA quantified at 260/280 nm with Thermo Scientific Nanodrop 2000 Spectrophotometer. First strand cDNA was

synthesized from 1µg of total RNA with reverse transcriptase (Thermofisher Scientific Verso cDNA synthesis kit) according to manufacturer instructions. Quantitative real time PCR was carried with SYBR green PCR master mix (Fermentas Life Sciences) on the ViiA7 instrument PCR system (Applied Biosystems, USA). The following cycling parameters were used: start at 95 °C for 5 min, denaturing at 95 °C for 30 s, annealing at 60 °C for 30 s, elongation at 72 °C for 30 s, and a final 5 min extra extension at the end of the reaction to ensure that all amplicons were completely extended and repeated for 40 amplification cycles. Relative quantification of expression of relevant genes was done using the ΔΔCt method after normalization to the expression of the housekeeping gene, GAPDH. The primer sequences used are given in Supp Table S1.

Western Blotting: Mesentery tissues were crushed in liquid nitrogen and 100 mg of tissue powder was added in 200 uL of RIPA lysis buffer (Merck, sigma 20-188). Homogenization was done on ice until a clear solution was obtained. After centrifuge for 20' at 12000 rpm, the supernatant was collected in a fresh microcentrifuge tube and incubated on ice for 30'. The protein content of tissue lysate was measured using the BCA kit (Thermofisher scientific, Massachusetts, USA). Protein samples were denatured at 95°C for 5' in Laemmli buffer. 60 ug of protein was loaded into each well and separated by 10% SDS-PAGE. The gel was run at 80 V for approximately 2 h. Proteins were electroblotted onto activated PVDF membrane at 60 V for 2 h at 4°C, and the membrane was blocked in 5% BSA in Tris-buffered saline containing 0.05% Tween for 2 h. Membranes were blotted with various primary antibodies i.e. VEGFC, VEGFR-3, Akt, p-Akt and GAPDH overnight at 4°C followed by the appropriate HRP-conjugated anti-rabbit and anti-mouse secondary antibody for 2 h. The membrane was then treated with

the chemiluminescence ECL, and visualized on gel doc (Invitrogen, iBrightCL1500). Densitometry was performed using standard NIH software (ImageJ). Details of the antibodies are given in Supp Table S2.

Patient studies

Patients were eligible for inclusion in this study if they had been diagnosed with liver cirrhosis (viral, alcoholic or NAFLD). The diagnosis of liver cirrhosis was established by means of histology and / or by its clinical, laboratory, endoscopic or imaging manifestations. The exclusion criteria were as follows: malignancy, diabetes mellitus, rheumatic diseases, tuberculosis, renal diseases, gastrointestinal diseases (e.g. celiac disease, inflammatory bowel disease, gastrointestinal bleeding in the last 4 weeks), intestinal surgery or INR > 2 (to avoid risk of bleeding during taking of biopsy). All subjects enrolled in the study underwent an upper gastrointestinal tract endoscopy, during which biopsies were obtained from the second portion of the duodenum (D2), distal to the ampulla of Vater. D2 biopsies were fixed in 10% neutral buffered formalin, embedded in paraffin, sectioned at 3-5 µm and stained with haematoxylin and eosin. In each sample, histologic features were studied, in a blind fashion, and recorded.

Study groups: The study was approved by the Ethics Committee of Institute of liver and biliary Sciences (No. ILBS/AC/2018/11252/3215). Written informed consent was obtained from all subjects enrolled in the study. Patients with cirrhosis were subsequently divided into two groups: patients with decompensated cirrhosis (n = 13) or compensated cirrhosis (n = 12). Classification in decompensated or compensated disease was based on the presence or absence of ascites. The control group comprised of healthy individuals

matched for age and sex, without any of the above-stated exclusion criteria, who underwent an upper gastrointestinal tract endoscopy without pathologic findings (n = 8).

Statistical Analysis: Continuous variables were expressed either as mean ± standard deviation for continuous distribution or as median values for skewed distribution. Continuous variables were compared between two groups using unpaired two-tailed student t-test or MannWhitney U test. Bar diagrams and dot plots were plotted using GraphPad Prism (version Prism 8.4.3; GraphPad Software, San Diego, CA, USA) and statistical analysis was done using SPSS Statistics (version 20.0, SPSS Inc., Chicago, IL, USA). A $p < 0.05$ was considered statistically significant.

All authors had access to the study data and had reviewed and approved the final manuscript.

Author contributions

SK and DMT provided the concept, planned the study, performed *in vivo* animal experiments; SK and DMT drafted and finalized the manuscript; PJ performed all *in vitro* experiments and western blots; IK and SR performed all histological and fluorescence based assays; AG and PR performed experiments with the VEGF-C plasmid; AY was involved with DMT in the PPVL study; AR provided all inputs in histological analysis; SM Shastry and VR gave the clinical inputs and planned the patient study; VN, SNRR and SB were involved in the preparation and characterization of the VEGF-C

nanocarriers; SKS was involved in planning the study, providing clinical inputs and editing of the manuscript. All authors approved the manuscript.

Acknowledgements

We are grateful to National Research and Development Council, Government of India for filing an Indian patent, "Nanoengineered VEGF-C Molecule Formulation for Cirrhosis and Portal Hypertension (Indian Patent File. App No. 202011049544)" free of cost.

References

1. Albillos A, de Gottardi A, Rescigno M. The gut-liver axis in liver disease: Pathophysiological basis for therapy. *Journal of Hepatology* 2020;72:558–577.
2. Miller MJ, Mcdole JR, Newberry RD. Microanatomy of the intestinal lymphatic system. Ann N Y Acad Sci;1207 . Epub ahead of print 2010. DOI: 10.1111/j.1749-6632.2010.05708.x.
3. Bernier-Latmani J, Petrova T V. Intestinal lymphatic vasculature: Structure, mechanisms and functions. *Nature Reviews Gastroenterology and Hepatology* 2017;14:510–526.
4. Hong JW, Park HE, Shin MJ, Shin YB, Yoon JA. Secondary lymphedema after intestinal tuberculosis: A case report. Ann Rehabil Med 2019;43:725–729.
5. Danese S. Role of the vascular and lymphatic endothelium in the pathogenesis of inflammatory bowel disease: "Brothers in arms." *Gut* 2011;60:998–1008.
6. Dunbar BS, Elk JR, Drake RE, Laine GA. Intestinal lymphatic flow during portal venous hypertension. Am J Physiol - Gastrointest Liver Physiol;257 . Epub ahead of print 1989. DOI: 10.1152/ajpgi.1989.257.1.g94.

7. Chung C, Iwakiri Y. The lymphatic vascular system in liver diseases: its role in ascites formation. *Clinical and molecular hepatology* 2013;19:99–104.

8. Ribera J, Pauta M, Melgar-Lesmes P, Tugues S, Fernández-Varo G, Held KF, Soria G, Tudela R, Planas AM, Fernández-Hernando C, Arroyo V, Jiménez W, Morales-Ruiz M. Increased nitric oxide production in lymphatic endothelial cells causes impairment of lymphatic drainage in cirrhotic rats. Gut 2013;62:138–145.

9. Nurmi H, Saharinen P, Zarkada G, Zheng W, Robciuc MR, Alitalo K. VEGF □C is required for intestinal lymphatic vessel maintenance and lipid absorption . EMBO Mol Med 2015;7:1418–1425.

10. Kyung EK, Sung HK, Gou YK. Lymphatic development in mouse small intestine. Dev Dyn 2007;236:2020–2025.

11. Güç E, Briquez PS, Foretay D, Fankhauser MA, Hubbell JA, Kilarski WW, Swartz MA. Local induction of lymphangiogenesis with engineered fibrin-binding VEGF-C promotes wound healing by increasing immune cell trafficking and matrix remodeling. Biomaterials 2017;131:160–175.

12. Bouta EM, Bell RD, Rahimi H, Xing L, Wood RW, Bingham CO, Ritchlin CT, Schwarz EM. Targeting lymphatic function as a novel therapeutic intervention for rheumatoid arthritis. *Nature Reviews Rheumatology* 2018;14:94–106.

13. Hagura A, Asai J, Maruyama K, Takenaka H, Kinoshita S, Katoh N. The VEGF-C/VEGFR3 signaling pathway contributes to resolving chronic skin inflammation by activating lymphatic vessel function. J Dermatol Sci 2014;73:135–141.

14. Hsu SJ, Zhang C, Jeong J, Lee S il, McConnell M, Utsumi T, Iwakiri Y. Enhanced Meningeal Lymphatic Drainage Ameliorates Neuroinflammation and Hepatic

Encephalopathy in Cirrhotic Rats. Gastroenterology 2021;160:1315-1329.e13.

15. Lohela M, Saaristo A, Veikkola T, Alitalo K. Lymphangiogenic growth factors, receptors and therapies. *Thrombosis and Haemostasis* 2003;90:167–184.

16. Aoki Y, Tosato G. Lymphatic regeneration: New insights from VEGFR-3 blockade. *Journal of the National Cancer Institute* 2005;97:2–3.

17. Schwager S, Renner S, Hemmerle T, Karaman S, Proulx ST, Fetz R, Golding-Ochsenbein AM, Probst P, Halin C, Neri D, Detmar M. Antibody-mediated delivery of VEGF-C potently reduces chronic skin inflammation. JCI insight;3 . Epub ahead of print December 6, 2018. DOI: 10.1172/jci.insight.124850.

18. Banerjee S, Pillai J. Solid lipid matrix mediated nanoarchitectonics for improved oral bioavailability of drugs. Expert Opin Drug Metab Toxicol 2019;15:499–515.

19. Banerjee S, Roy S, Bhaumik KN, Pillai J. Mechanisms of the effectiveness of lipid nanoparticle formulations loaded with anti-tubercular drugs combinations toward overcoming drug bioavailability in tuberculosis. J Drug Target 2020;28:55–69.

20. Deng Y, Zhang X, Simons M. Molecular controls of lymphatic VEGFR3 signaling. Arterioscler Thromb Vasc Biol 2015;35:421–429.

21. D'Alessio S, Correale C, Tacconi C, Gandelli A, Pietrogrande G, Vetrano S, Genua M, Arena V, Spinelli A, Peyrin-Biroulet L, Fiocchi C, Danese S. VEGF-C-dependent stimulation of lymphatic function ameliorates experimental inflammatory bowel disease. J Clin Invest 2014;124:3863–3878.

22. Visuri MT, Honkonen KM, Hartiala P, Tervala T V., Halonen PJ, Junkkari H, Knuutinen N, Ylä-Herttuala S, Alitalo KK, Saarikko AM. VEGF-C and VEGF-C156S in the pro-lymphangiogenic growth factor therapy of lymphedema: a large

animal study. Angiogenesis 2015;18:313–326.

23. Cabrera J, Falcón L, Gorriz E, Pardo MD, Granados R, Quinones A, Maynar M. Abdominal decompression plays a major role in early postparacentesis haemodynamic changes in cirrhotic patients with tense ascites. Gut 2001;48:384–389.

24. Aukland K, Reed RK. Interstitial-lymphatic mechanisms in the control of extracellular fluid volume. Physiol Rev 1993;73:1–78.

25. Geerts AM, De Vriese AS, Vanheule E, Van Vlierberghe H, Mortier S, Cheung KJ, Demetter P, Lameire N, De Vos M, Colle I. Increased angiogenesis and permeability in the mesenteric microvasculature of rats with cirrhosis and portal hypertension: An in vivo study. Liver Int 2006;26:889–898.

26. Chakraborty S, Zawieja SD, Wang W, Lee Y, Wang YJ, Von Der Weid PY, Zawieja DC, Muthuchamy M. Lipopolysaccharide modulates neutrophil recruitment and macrophage polarization on lymphatic vessels and impairs lymphatic function in rat mesentery. Am J Physiol - Hear Circ Physiol 2015;309:H2042–H2057.

27. Torrisi JS, Hespe GE, Cuzzone DA, Savetsky IL, Nitti MD, Gardenier JC, Nores GDG, Jowhar D, Kataru RP, Mehrara BJ. Inhibition of Inflammation and iNOS Improves Lymphatic Function in Obesity. Sci Rep;6 . Epub ahead of print January 22, 2016. DOI: 10.1038/srep19817.

28. Vieira JM, Norman S, Del Campo CV, Cahill TJ, Barnette DN, Gunadasa-Rohling M, Johnson LA, Greaves DR, Carr CA, Jackson DG, Riley PR. The cardiac lymphatic system stimulates resolution of inflammation following myocardial

infarction. J Clin Invest 2018;128:3402–3412.

29. Coso S, Zeng Y, Opeskin K, Williams ED. Vascular endothelial growth factor receptor-3 directly interacts with phosphatidylinositol 3-kinase to regulate lymphangiogenesis. PLoS One;7 . Epub ahead of print June 22, 2012. DOI: 10.1371/journal.pone.0039558.

30. Hagendoorn J, Padera TP, Kashiwagi S, Isaka N, Noda F, Lin MI, Huang PL, Sessa WC, Fukumura D, Jain RK. Endothelial nitric oxide synthase regulates microlymphatic flow via collecting lymphatics. Circ Res 2004;95:204–209.

31. Bosch J, Gracia-Sancho J, Abraldes JG. Cirrhosis as new indication for statins. Gut 2020;69:953–962.

32. Vignes S, Bellanger J. Primary intestinal lymphangiectasia (Waldmann's disease). Orphanet J Rare Dis;3 . Epub ahead of print 2008. DOI: 10.1186/1750-1172-3-5.

33. Rahier JF, De Beauce S, Dubuquoy L, Erdual E, Colombel JF, Jouret-Mourin A, Geboes K, Desreumaux P. Increased lymphatic vessel density and lymphangiogenesis in inflammatory bowel disease. Aliment Pharmacol Ther 2011;34:533–543.

34. Linares PM, Gisbert JP. Role of growth factors in the development of lymphangiogenesis driven by inflammatory bowel disease: A review. *Inflammatory Bowel Diseases* 2011;17:1814–1821.

35. Tripathi DM, Vilaseca M, Lafoz E, Garcia-Calderó H, Viegas Haute G, Fernández-Iglesias A, Rodrigues de Oliveira J, García-Pagán JC, Bosch J, Gracia-Sancho J. Simvastatin Prevents Progression of Acute on Chronic Liver Failure in Rats With Cirrhosis and Portal Hypertension. Gastroenterology 2018;155:1564–

1577.

Table 1: Characteristics of patients used in the study

Parameters	**Decompensated (12)**	**Compensated (11)**	**Controls (8)**
Age (mean±SD, yr.)	53.8 ± 9.25	55.4 ± 10.01	52 ± 11.3
Gender	9M, 4F	9M, 3F	5M, 3F
Aetiology of cirrhosis (Alcohol/NASH/Viral)	4/8/1	2/9/1	-
INR	1.8 ± 0.5	1.3 ± 0.2	1.1 ± 0.2
Serum albumin (g/dL)	3.0 + 0.3	3.2 + 0.49	4.2 + 0.19
Total bilirubin (mg／dL)	2.68 ± 1.1	1.32 ± 0.5	0.8 ± 0.4
Platelets	108.3 ± 50.9	136.4 ± 64.8	213 ± 61.5
Presence of Ascites (n/n)	13/13	0/12	-
MELD-Na Score	20.23 ± 1.8	10.9 ± 1.99	-

INR: international normalized ratio; MELD: Model for End-Stage Liver Disease

Figure Legends

Figure 1: **Properties of nanoengineered VEGF-C (E-VEGF-C).** (A) A schematic representation of vegfr3-tagged VEGF-C nano-lipocarriers (E-VEGF-C). (B) Mean particle size of E-VEGF-C immunolipo-nanocarriers (C) Mean zeta potential value of E-VEGF-C immunolipo-nanocarriers without vegfr3 antibody (D) Mean zeta potential value with vegfr3 antibody. Different coloured peaks in the graphs are representing different replicates of samples. (E) SEM analysis of E-VEGF-C immunolipo-nanocarriers after incubation with vegfr3 antibody. (F) TEM analysis of E-VEGF-C after incubation with vegfr3 antibody.

Figure 2: Invitro studies of lymphatic endothelial cells (LyECs) with E-VEGF-C. (A) Culture of Podoplanin positive (Pdpn+) LyECs after flow sorting. (B) Fluorescent images (20x) showing Pdpn positivity of the sorted LyECs. (C) Fluorescent images showing uptake of coumarin-6 labeled E-VEGF-C by LyECs at 60 min and 240 min. Scale bars depict 100µm. (D) Line graph depicting the percentage of coumarin-positive cells (flourescence) at different time points.

Figure 3: *In vivo* biodistribution studies after 2 hours of E-VEGF-C treatment. (A) Schema of *in vivo* biodistribution studies. (B) Representative flourescence images of E-VEGF-C treated CCl4 rats showing co-localization of coumarin-6 labelled nanoparticles (C-NPs) and pdpn-positive lymphatic vessels in the mesentery. Scale bars depict 200µm. (C) Human VEGF-C levels (pg/mg total protein) in different tissues in control and CCl4

animals. (D) Levels of human VEGF-C (pg/ml) in rat plasma samples at indicated time points in CCl4 rats. Data represents mean ± standard deviation. N=4 each. '*' represents $p < 0.05$ and '**' represents $p < 0.001$.

Figure 4: Effect of E-VEGF-C treatment on mesenteric lymphatic vessels in cirrhotic animal models of portal hypertension. (A) Schema of the *in vivo* studies. (B) Pdpn+ immunohistochemistry in the mesenteric tissue sections of control, CCl4-V and E-VEGFC treated rat. Scale bars represent 200µm. (C) Bar diagrams showing average number of pdpn+ cells per field in the study groups. Data represents mean ± standard deviation. N=5 each. (D) Representative fluorescent images of vegfr3 positive lymphatic channels in the mesenteric tissues of CCl4-V and E-VEGF-C rats. Nuclei were stained with DAPI. Scale bars depict 100µm. (E) Bar diagrams showing the average number of vegfr3 positive lymphatic vessels in the mesentery of different study groups. Data represents mean ± standard deviation. N=5 each. (F) Expression of different proteins in the mesenteric tissues of control, CCl4-V and E-VEGF-C treated rats as determined by Western blots and normalized to GAPDH. Dotted line indicates control. Data represents mean ± standard deviation. N=4 each. '*' represents $p < 0.05$ versus control. '#' represents $p < 0.05$ versus CCl4 vehicle. (G) Confocal images showing bodipy labeling in the mesenteric lymphatic channels. Images were taken after 2h of oral administration of bodipy. Scale bars depict 20µm. (H) Bar diagram depicting normailzed fluorescence intensity in CCl4-V and E-VEGF-C rats. Data represents mean ± standard deviation. N=4 each. '*' represents $p < 0.05$, '**' represents $p < 0.001$.

Figure 5: Effect of E-VEGF-C treatment on ascitic fluid and liver physiology in cirrhotic animal models of portal hypertension. (A) Representative computed tomographic (CT) scan slices showing abdominal cavity of the study groups. The regions of interest are marked with red dotted outline and correspond to the zones with accumulation of liquid. (B) Dot plots showing ascitic fluid volume (ml) in the study groups. Horizontal bars represent median values. (C) Bar diagrams showing plasma volumes (ml) in the study groups measured using the Evans Blue dye dilution technique. Data represents mean ± standard deviation. N=4 each. (D) Bar Diagrams showing hepatic hemodynamic parameters, Portal pressure (PP), Portal Blood Flow (PBF) and Intrahepatic resistance (IHR) in the control, CCl4-V cirrhotic and E-VEGF-C rats. Data represents mean ± standard deviation. N=6 each. (E) Masson Trichrome stained images of liver tissues in controls, CCl4-V and E-VEGF-C rats. Liver fibrosis was assessed using Ishak's fibrosis scoring system. Scale bars depict 200µm. (F) Relative expression of genes in CCl4-V and E-VEGF-C rats with respect to controls in the mesenteric tissues. Data represents mean ± standard deviation. N=4 each. '*' represents $p < 0.05$ and '**' represents $p < 0.001$.

Figure 6: Effect of E-VEGF-C treatment on mesenteric lymphatic vessels and liver physiology in the non-cirrhotic animal models of portal hypertension. (A) Schema of the studies (B) Vegfr3+ immunohistochemistry in the mesenteric tissue sections of PPVL-VEH and PPVL + E-VEGF-C rats. Scale bars depict 200µm. (C) Bar diagrams showing the average number of vegfr3 positive lymphatic vessels. Data represents mean ± standard deviation. N=5 each. (D) Expression of different proteins in the mesenteric

tissues of control, PPVL-VEH and PPVL + E-VEGF-C treated rats as determined by Western blot and normalized to GAPDH. Dotted line indicates control. Data represents mean ± standard deviation. N=4 each. '*' represents $p < 0.05$ and '**' represents $p < 0.001$ versus control. '#' represents $p < 0.05$ versus CCl4 vehicle. (E) Bar Diagrams showing hepatic hemodynamic parameters, Portal pressure (PP), Portal Blood Flow (PBF) and Intrahepatic resistance (IHR) in the non-cirrhotic PPVL rats treated with vehicle and that treated with E-VEGF-C. Data represents mean ± standard deviation. N=6 each. (F) Relative expression of genes in PPVL-VEH and PPVL + E-VEGF-C rats with respect to controls in the mesenteric tissues. Data represents mean ± standard deviation. N=4 each. '*' represents $p < 0.05$ and '**' represents $p < 0.001$.

Figure 7: Duodenal lymphatic channels in cirrhotic patients (A) Representative vegfr3 and pdpn immunohistochemical (IHC) stained sections of duodenal (D2) biopsies in patients with compensated cirrhosis and decompensated cirrhosis. Lymphatic vessels are shown by dotted lines. Scale bars depict 100μm. (B, C) Dot plots showing average number of vegfr3 and pdpn-positive lymphatic vessels per field in the study groups. Horizontal bars represent median values. (D) Bar diagrams showing average diameter of vegfr3-positive lymphatic vessels per field in the study groups (n=8 each). Data represents mean ± standard deviation. '*' represents $p < 0.05$ and '**' represents $p < 0.001$.

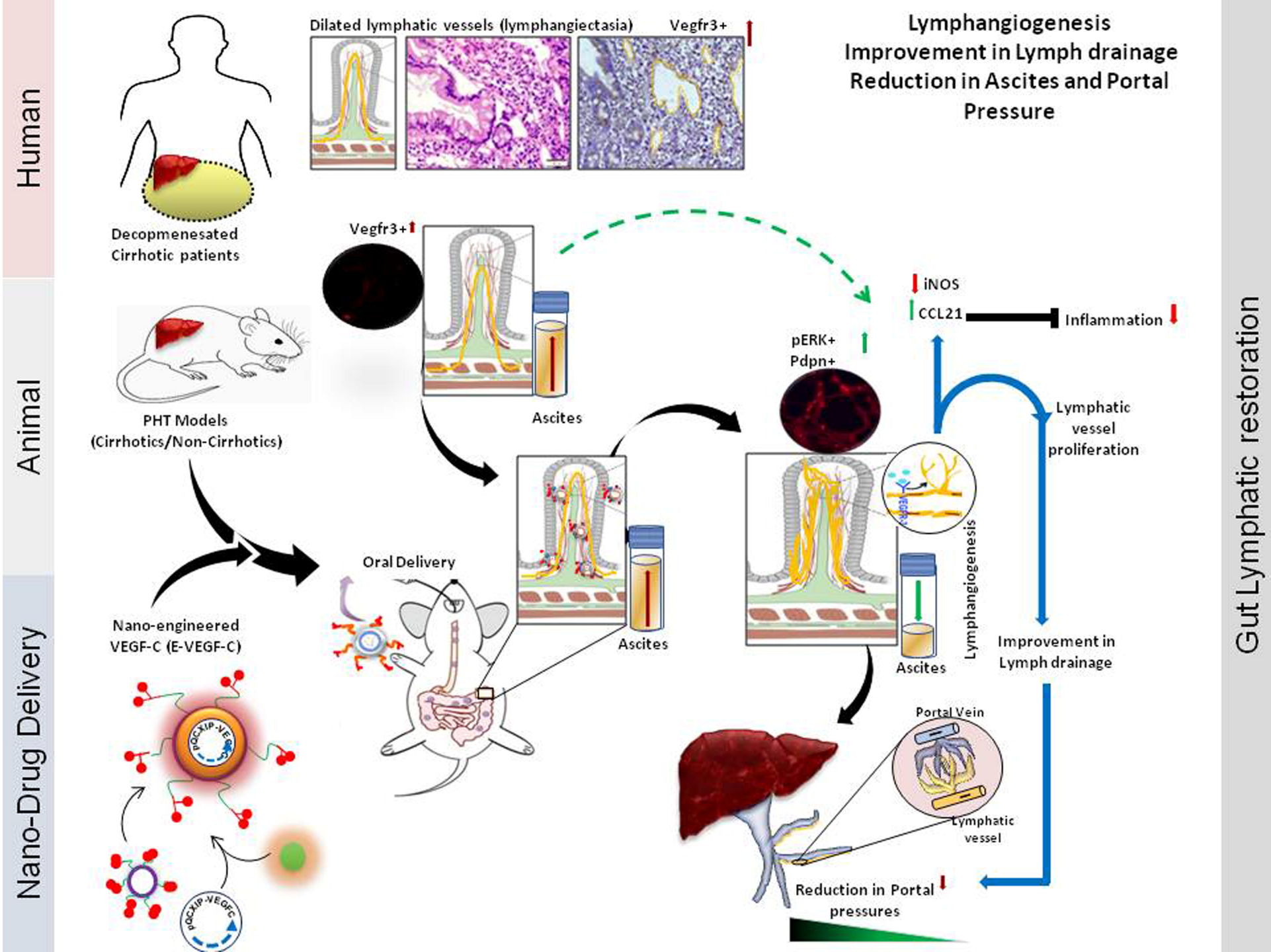
Human
Animal
Nano-Drug Delivery
Gut Lymphatic restoration
Lymphangiogenesis
Improvement in Lymph drainage
Reduction in Ascites and Portal Pressure
Dilated lymphatic vessels (lymphangiectasia)
Vegfr3+
Decopmenesated Cirrhotic patients
PHT Models (Cirrhotics/Non-Cirrhotics)
Nano-engineered VEGF-C (E-VEGF-C)
Oral Delivery
Ascites
iNOS
CCL21
Inflammation
pERK+
Pdpn+
Lymphatic vessel proliferation
Lymphangiogenesis
Improvement in Lymph drainage
Portal Vein
Lymphatic vessel
Reduction in Portal pressures

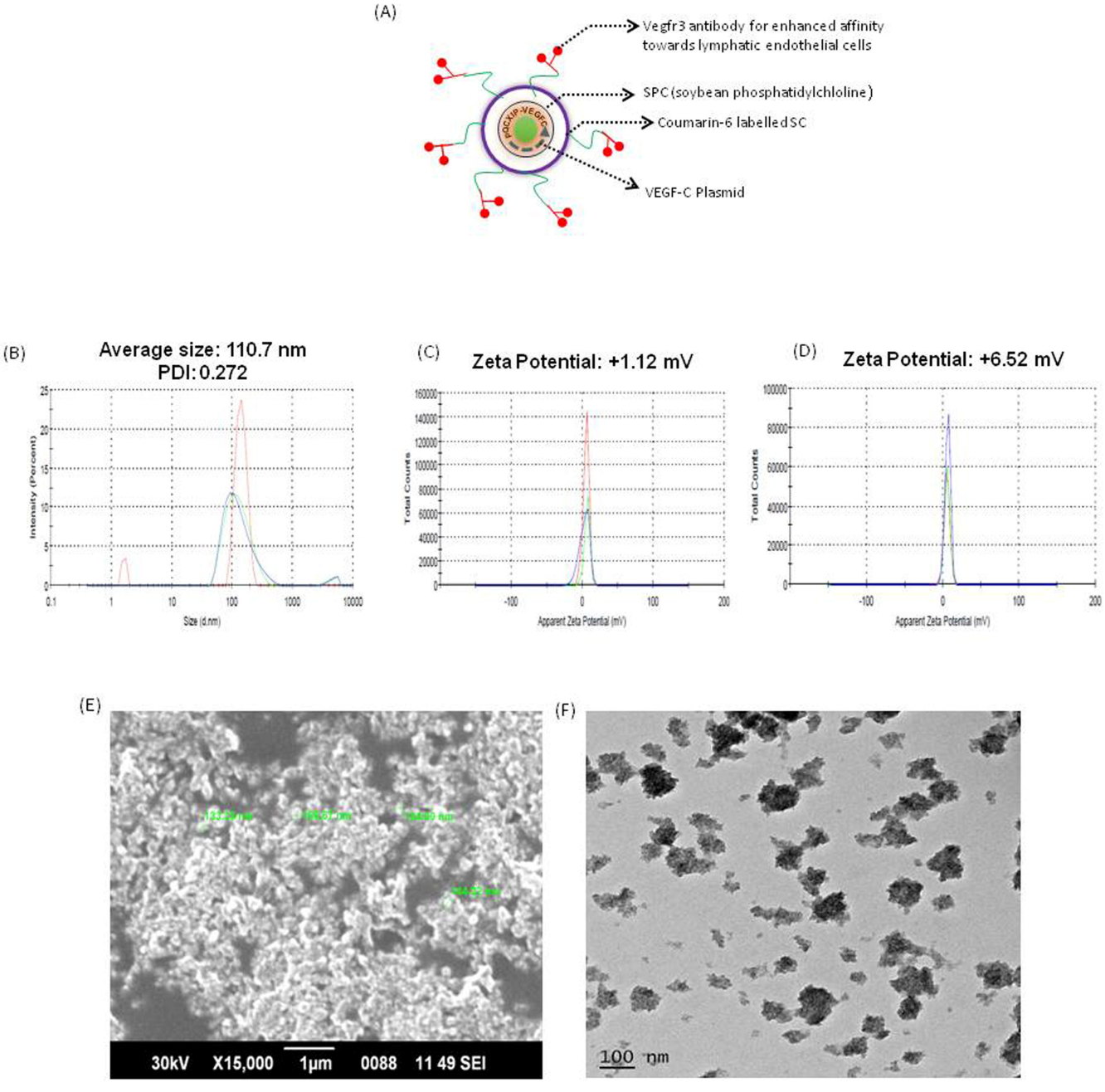
(A)
Vegfr3 antibody for enhanced affinity towards lymphatic endothelial cells
SPC (soybean phosphatidylchloline)
Coumarin-6 labelled SC
VEGF-C Plasmid
(B)
Average size: 110.7 nm
PDI: 0.272
Intensity (Percent)
Size (d.nm)
(C)
Zeta Potential: +1.12 mV
Total Counts
Apparent Zeta Potential (mV)
(D)
Zeta Potential: +6.52 mV
Total Counts
Apparent Zeta Potential (mV)
(E)
30kV X15,000 1μm 0088 11 49 SEI
(F)
100 nm

(A)

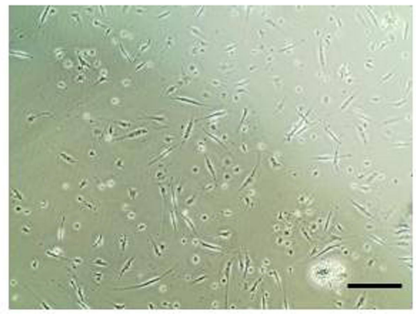

(B)

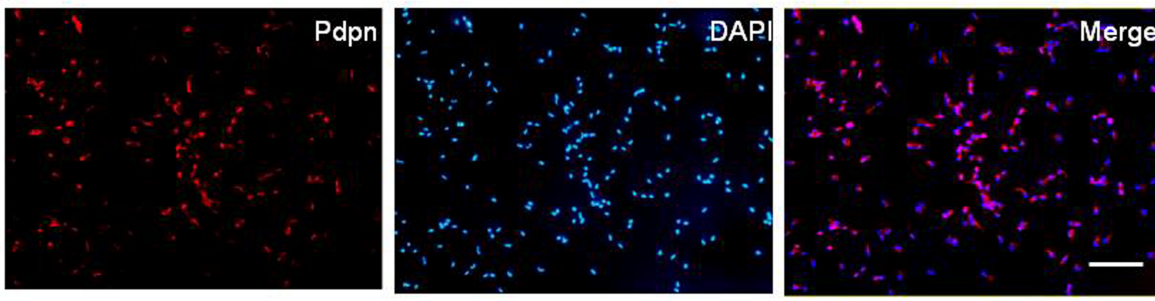
Pdpn
DAPI
Merge

(C)

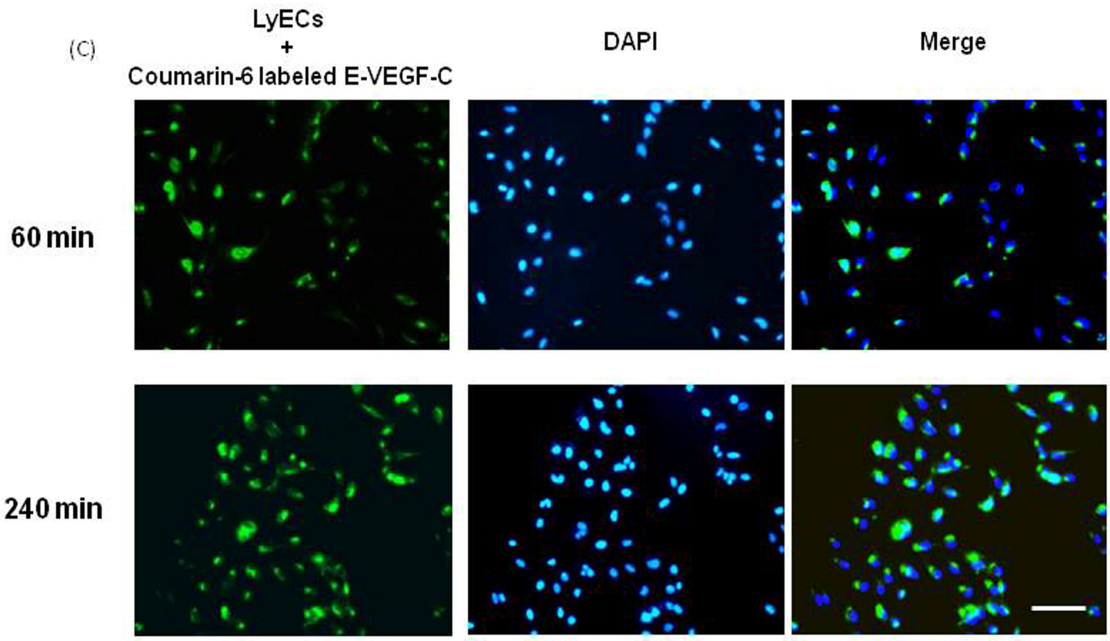
LyECs
+
Coumarin-6 labeled E-VEGF-C
DAPI
Merge
60 min
240 min

(D)

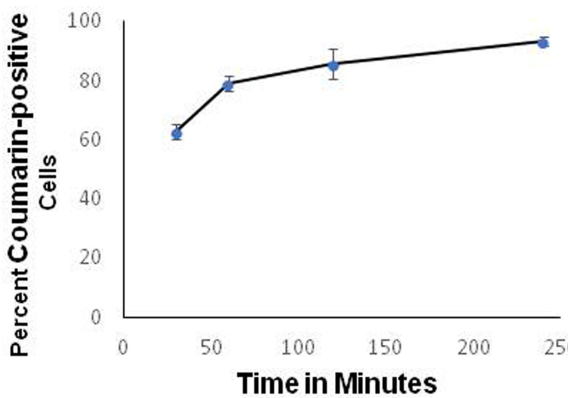
Percent Coumarin-positive Cells
100
80
60
40
20
0
0
50
100
150
200
250
Time in Minutes

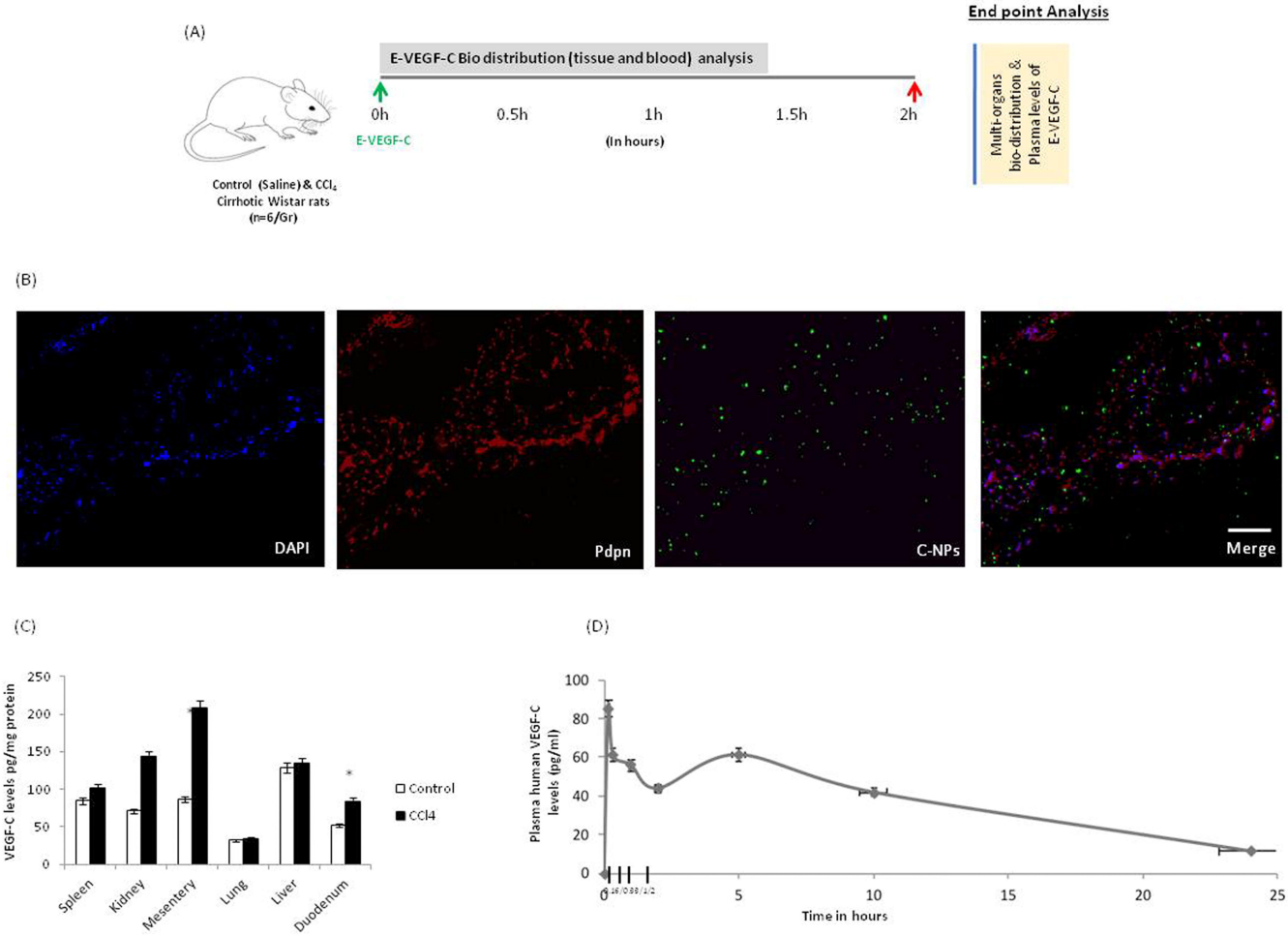
(A)
End point Analysis
E-VEGF-C Bio distribution (tissue and blood) analysis
0h
0.5h
1h
1.5h
2h
E-VEGF-C
(In hours)
Multi-organs bio-distribution & Plasma levels of E-VEGF-C
Control (Saline) & CCl4 Cirrhotic Wistar rats (n=6/Gr)
(B)
DAPI
Pdpn
C-NPs
Merge
(C)
VEGF-C levels pg/mg protein
250
200
150
100
50
0
Control
CCl4
Spleen
Kidney
Mesentery
Lung
Liver
Duodenum
(D)
Plasma human VEGF-C levels (pg/ml)
100
80
60
40
20
0
5
10
15
20
25
Time in hours

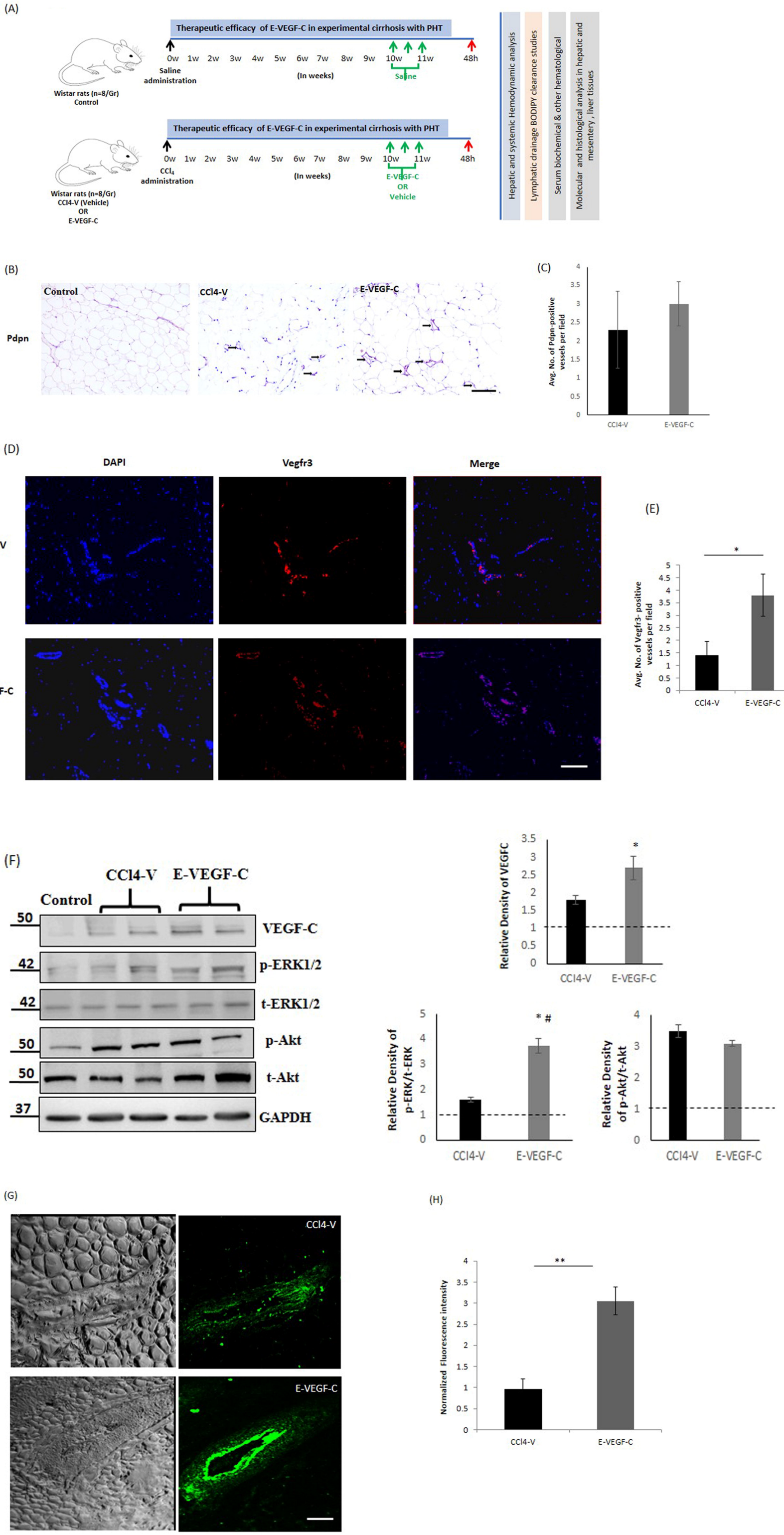
(A)
Therapeutic efficacy of E-VEGF-C in experimental cirrhosis with PHT
0w 1w 2w 3w 4w 5w 6w 7w 8w 9w 10w 11w 48h
Saline administration
(In weeks)
Saline
Wistar rats (n=8/Gr) Control
Therapeutic efficacy of E-VEGF-C in experimental cirrhosis with PHT
0w 1w 2w 3w 4w 5w 6w 7w 8w 9w 10w 11w 48h
CCl4 administration
(In weeks)
E-VEGF-C OR Vehicle
Wistar rats (n=8/Gr) CCl4-V (Vehicle) OR E-VEGF-C
Hepatic and systemic Hemodynamic analysis
Lymphatic drainage BODIPY clearance studies
Serum biochemical & other hematological
Molecular and histological analysis in hepatic and mesentery , liver tissues
(B)
Control
CCl4-V
E-VEGF-C
Pdpn
(C)
Avg. No. of Pdpn-positive vessels per field
CCl4-V
E-VEGF-C
(D)
DAPI
Vegfr3
Merge
CCl4-V
E-VEGF-C
(E)
Avg. No. of Vegfr3- positive vessels per field
CCl4-V
E-VEGF-C
(F)
CCl4-V
E-VEGF-C
Control
50
VEGF-C
42
p-ERK1/2
42
t-ERK1/2
50
p-Akt
50
t-Akt
37
GAPDH
Relative Density of VEGFC
CCl4-V
E-VEGF-C
Relative Density of p-ERK/t-ERK
Relative Density of p-Akt/t-Akt
(G)
CCl4-V
E-VEGF-C
(H)
Normalized Fluorescence intensity
CCl4-V
E-VEGF-C

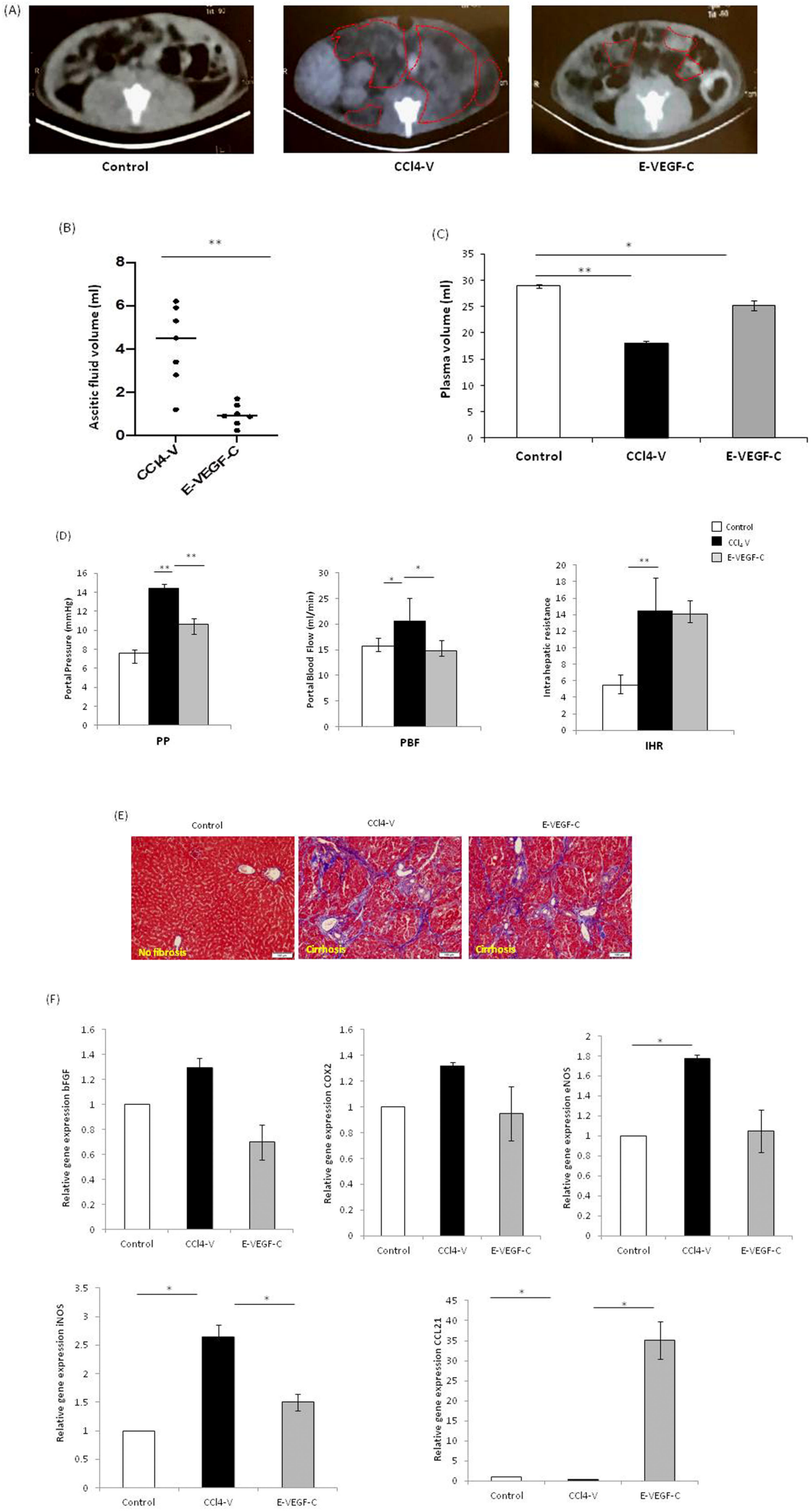
(A)
Control
CCl4-V
E-VEGF-C
(B)
Ascitic fluid volume (ml)
CCl4-V
E-VEGF-C
(C)
Plasma volume (ml)
Control
CCl4-V
E-VEGF-C
(D)
Control
CCl4 V
E-VEGF-C
Portal Pressure (mmHg)
PP
Portal Blood Flow (ml/min)
PBF
Intra hepatic resistance
IHR
(E)
Control
CCl4-V
E-VEGF-C
No fibrosis
Cirrhosis
Cirrhosis
(F)
Relative gene expression bFGF
Relative gene expression COX2
Relative gene expression eNOS
Relative gene expression iNOS
Relative gene expression CCL21
Control
CCl4-V
E-VEGF-C

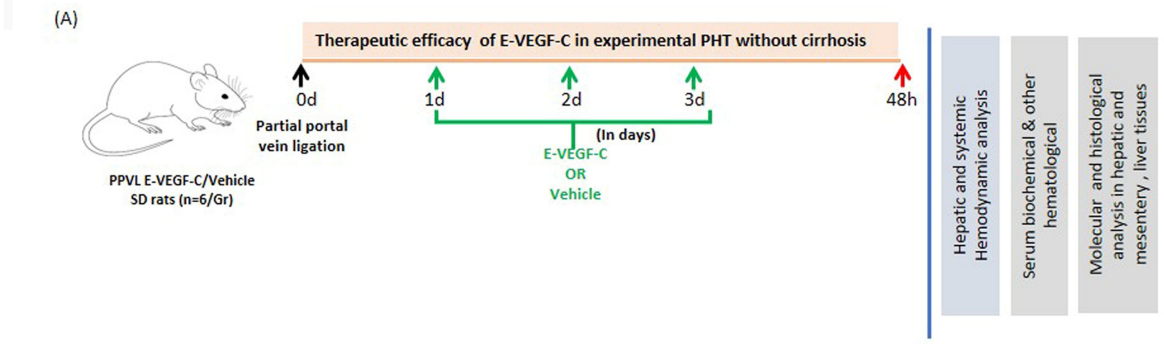
(A)
Therapeutic efficacy of E-VEGF-C in experimental PHT without cirrhosis
0d
1d
2d
3d
48h
Partial portal vein ligation
(In days)
E-VEGF-C
OR
Vehicle
PPVL E-VEGF-C/Vehicle
SD rats (n=6/Gr)
Hepatic and systemic Hemodynamic analysis
Serum biochemical & other hematological
Molecular and histological analysis in hepatic and mesentery , liver tissues

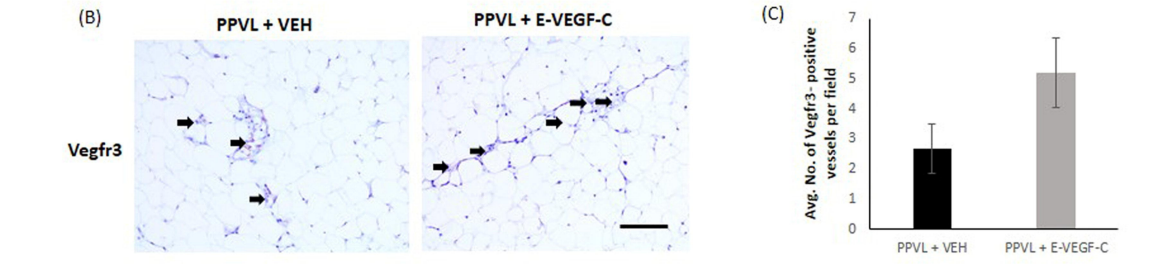
(B)
PPVL + VEH
PPVL + E-VEGF-C
Vegfr3
(C)
Avg. No. of Vegfr3- positive vessels per field
PPVL + VEH
PPVL + E-VEGF-C

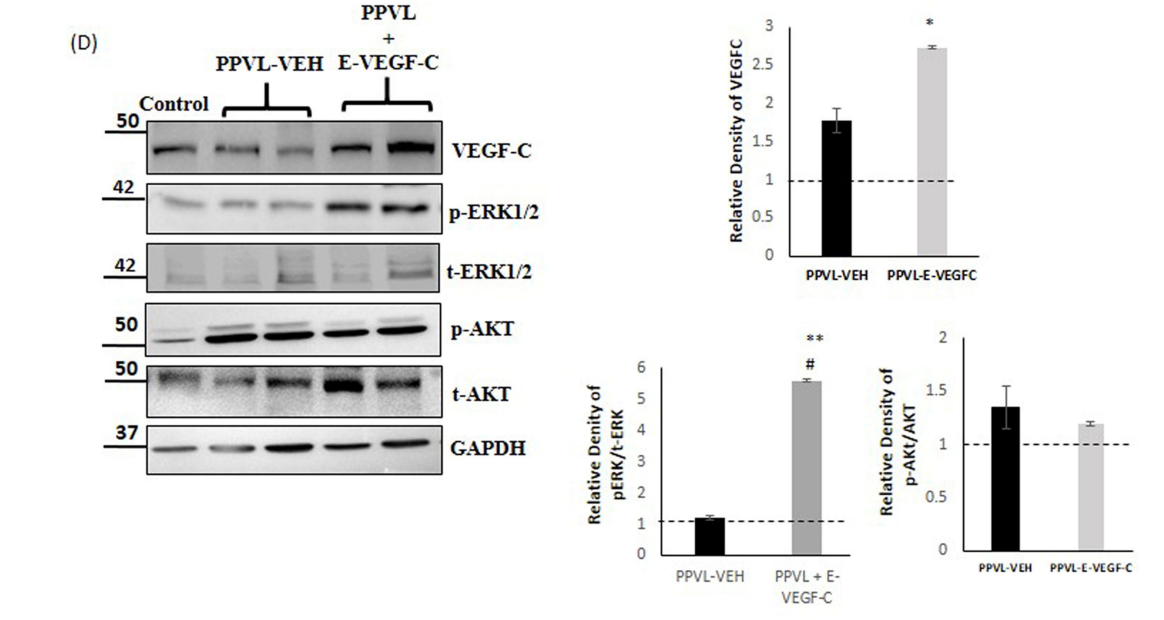
(D)
PPVL
+
PPVL-VEH
E-VEGF-C
Control
50
VEGF-C
42
p-ERK1/2
42
t-ERK1/2
50
p-AKT
50
t-AKT
37
GAPDH
Relative Density of VEGFC
PPVL-VEH
PPVL-E-VEGFC
Relative Denity of pERK/t-ERK
PPVL-VEH
PPVL + E-VEGF-C
Relative Density of p-AKt/AKT
PPVL-VEH
PPVL-E-VEGF-C

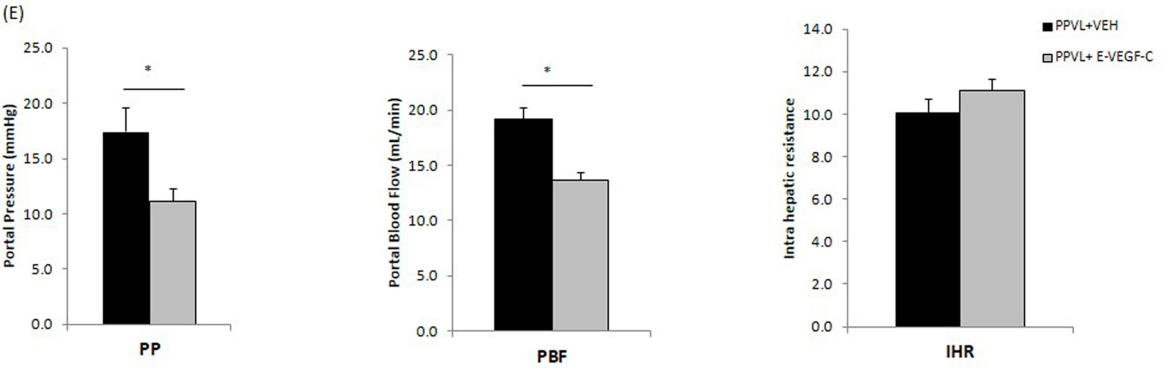
(E)
Portal Pressure (mmHg)
PP
Portal Blood Flow (mL/min)
PBF
Intra hepatic resistance
IHR
PPVL+VEH
PPVL+ E-VEGF-C

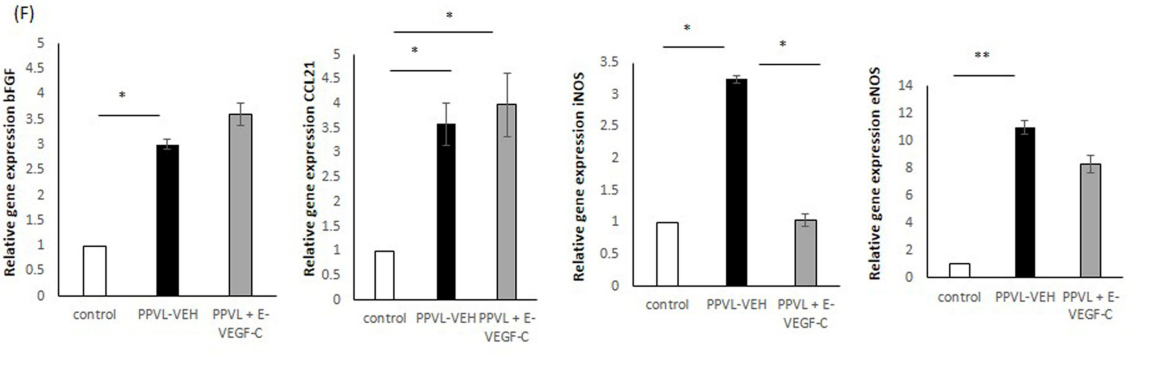
(F)
Relative gene expression bFGF
Relative gene expression CCL21
Relative gene expression iNOS
Relative gene expression eNOS
control
PPVL-VEH
PPVL + E-VEGF-C

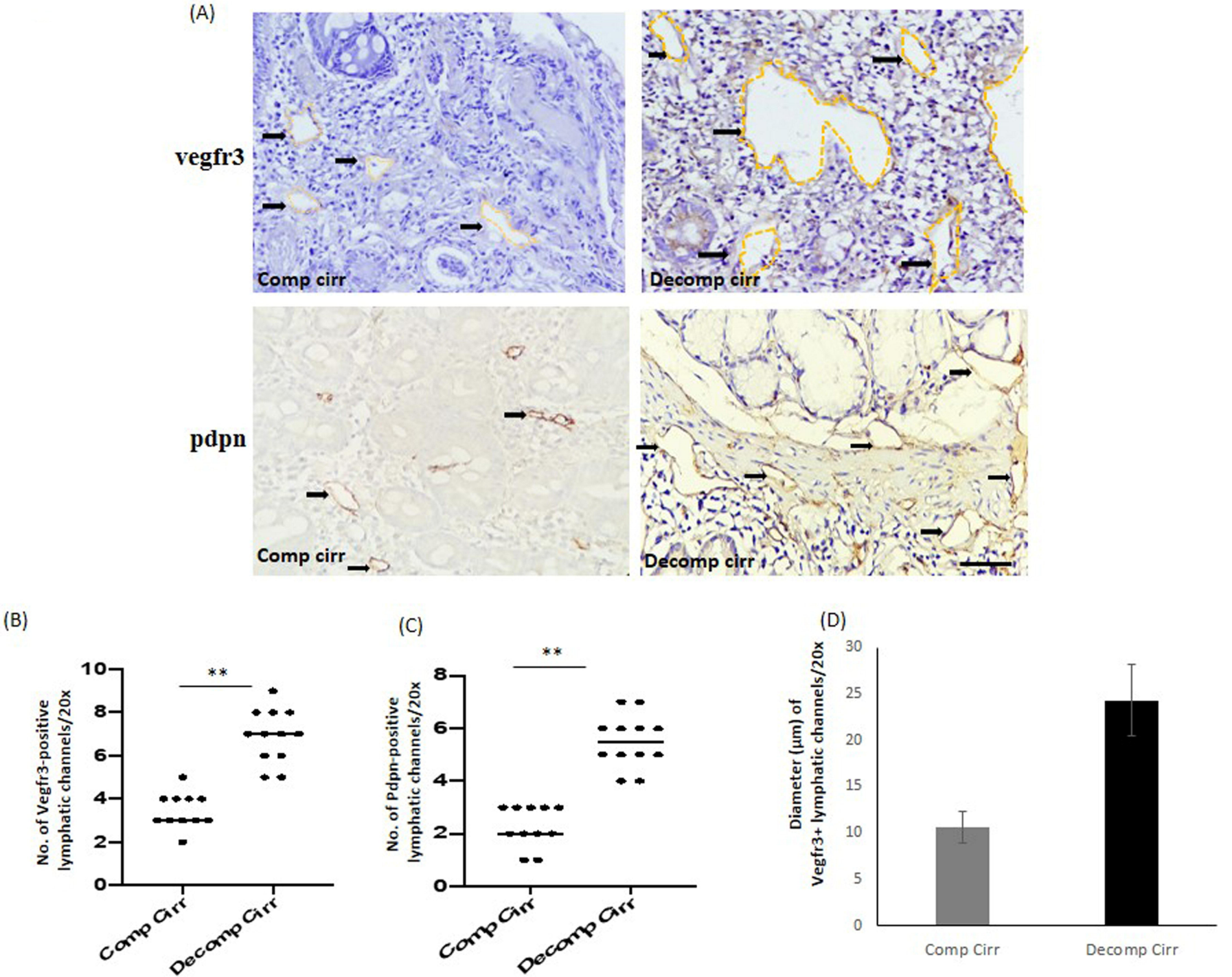
(A)
vegfr3
pdpn
Comp cirr
Decomp cirr
Comp cirr
Decomp cirr
(B)
No. of Vegfr3-positive lymphatic channels/20x
**
Comp Cirr
Decomp Cirr
(C)
No. of Pdpn-positive lymphatic channels/20x
**
Comp Cirr
Decomp Cirr
(D)
Diameter (µm) of Vegfr3+ lymphatic channels/20x
Comp Cirr
Decomp Cirr